Journal of Sound and Vibration (1999) **219**(4), 581–601
Article No. jsvi.1998.1926, available online at http://www.idealibrary.com.on IDEAL

THE SCATTERING AT A CORNER WITH ABSORBING FLANKS AND AN ABSORBING CYLINDER

F. P. MECHEL
D-71120 *Grafenau* 1, *Germany*

(*Received* 11 *June* 1998)

This paper continues and terminates the sequence of the preceding papers [1–4] about sound fields in wedge-shaped spaces, and especially resumes the topic of reference [4] which deals with the scattering of sound at building corners and an absorbing cylinder which surrounds the corner. The corner flanks in [4] were supposed to be rigid, so the sound field could be synthesized with ideal wedge modes. The present paper continues the task of reference [4], but now the corner flanks are absorbing. A model of the arrangement is applied which uses a special case of the modal analysis in reference [1]. The field space is subdivided into ring-shaped zones with radii r_i, and the wall admittance G_i of the absorbing flank in each zone is supposed to be inversely proportional to the radius, $G_i(r) \sim 1/r$, so that the average value of the model admittance in a zone $\langle G_i(r) \rangle$ equals the admittance G of the flank. An admittance function $G_i(r) \sim 1/r$ is associated with wedge modes of a simple form. The model with the "stepping admittance flank" is an approximate to the corner with constant admittance if the number of ring-shaped zones is high enough, so that the variation of $G_i(r)$ in the zones remains restricted. The absorbing cylinder around the corner is used here for two reasons: first, the stepping admittance model is singular at the corner, which is excluded by the cylinder, second: it shall be investigated how an absorbing flank will influence the potential of the cylinder to improve the corner shielding which was demonstrated in reference [4] for rigid corner flanks.

1. INTRODUCTION

The present paper is a member of a series of previous papers [1–4], which all have as their common topic the sound field analysis in wedge-shaped spaces. The common aim is the field synthesis with wedge modes, which are mutually orthogonal between the wedge flanks. The last contribution [4] dealt with the sound scattering at rigid corners which are surrounded by an absorbing cylinder. The rigid corner flanks allow for the use of "ideal wedge modes" (associated with ideally reflecting flanks) for the field formulation. The first contribution [1] explained (with literature about the theme), why special problems are encountered when the flanks of the wedge-shaped space are absorbing; then the wave equation in cylinder co-ordinates generally is no longer separable. A special condition was

0022–460X/99/040581 + 21 $30.00/0

indicated in reference [1] for which the separability is retained even with absorbing flanks, namely when the (normalized) surface admittance G of the flank is a radial function $G(r) \sim 1/r$ inversely proportional to the radius r. The radial functions of the wedge modes then are Bessel, Neumann or Hankel functions with complex orders. This special case is used here to construct a model of the corner with a locally absorbing flank having a constant surface admittance G.

The philosophy of the model makes use of the general finding that reflection and scattering at absorbing walls or sound propagation along walls with "structured" (i.e., spatially variable) admittance can be approximated by interactions with a wall with constant admittance if, first, the variation of the admittance is not too strong, and second if the structure dimensions are small compared to the wave length. Then the average admittance is the important quantity. Therefore one can subdivide the wedge space into ring-shaped zones with radii r_i and suppose in each zone a flank admittance $G_i(r) = c_i/r$. The factors c_i are determined so that the average $\langle G_i(r) \rangle$ over the width Δr of the ring equals G. One easily finds

$$G_i(r) = \frac{G}{r} \frac{r_i - r_{i-1}}{\ln (r_i/r_{i-1})}. \tag{1}$$

A typical arrangement is illustrated in Figure 1(a). A corner with one rigid and one absorbing flank lets a wedge-shaped field space with a wedge angle Θ_0 (e.g.,

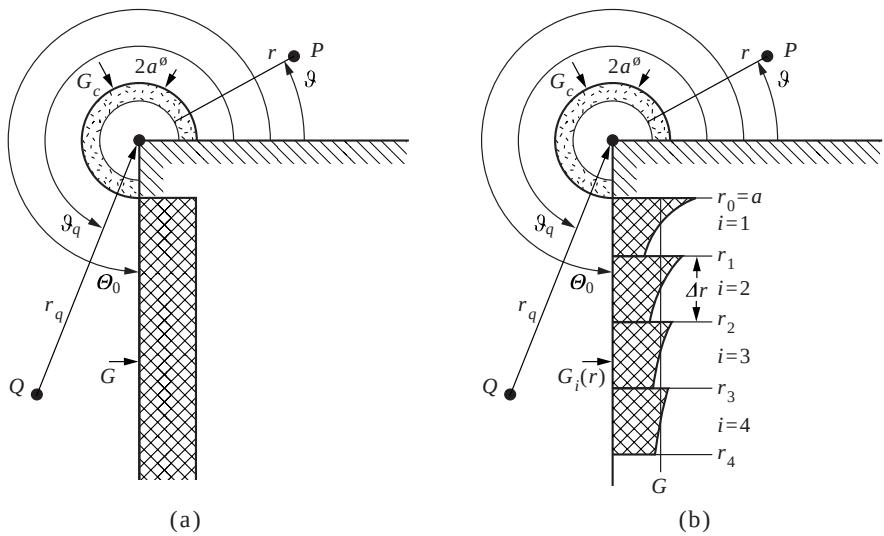

Figure 1. (a) Scheme of a corner with one rigid flank (at $\vartheta = 0$) and one absorbing flank (at $\vartheta = \Theta_0$) with an absorbing cylinder of radius a and a (normalized) surface admittance G_c. A line source is at $Q = (r_q, \vartheta_q)$. (b) Scheme of the stepped admittance model of a corner with one rigid flank (at $\vartheta = 0$) and one absorbing flank (at $\vartheta = \Theta_0$).

$\Theta_0 = 270^\circ$ in the sketch). The corner is surrounded by a cylinder of radius a which is supposed to be locally absorbing with a (normalized) surface admittance G_c. Two types are considered for the incident sound. In the first case it is produced by a line source (parallel to the corner) at position Q with the coordinates (r_q, ϑ_q). One can then place the source inside one of the ring zones, $r_{s-1} < r_q < r_s$, with a zone number $i = s$. The second case with an incident plane wave is obtained by letting $r_q \to \infty$. Figure 1(b) shows the scheme of the stepping wall admittance $G_i(r)$ at the absorbing flank. The admittance steps between the zones become smaller and smaller with increasing zone limit radius r_i. Except near the origin they can be made small by choosing small Δr values. Note that Δr must not be constant; it could be set to smaller values near to the origin and to larger values in greater distances. The absorbing cylinder with radial surface admittance G_c and diameter $2a$ eliminates the singularity at the origin.

The example of Figure 1 (with the arbitrary value $\Theta_0 = 270^\circ$) with an ideal and an absorbing flank is an element of the more general case that both flanks are absorbing. Then the ideal flank is placed in the angle bisector of the wedge angle, and the ideal flank is rigid, if the sound field is symmetrical with respect to the angle bisector (e.g., the line source lying on it or the plane wave incident parallel to it). For more general source positions the task is solved twice: first with a rigid flank in the angle bisector, then with a soft (pressure release) flank at the angle bisector. Any skew field distribution then can be represented by a superposition of these solutions. Here the main concern is with the arrangement of one rigid and one absorbing flank. The most important intermediate results for a soft flank combined with an absorbing flank will be given, however.

Any wedge angle $0 < \Theta_0 \leqslant 2\pi$ is possible. The results of the present stepped admittance model can be checked with results from other models and theories. If the wedge angle is moderate, $\Theta_0 \leqslant 45^\circ$, the results of the present method can be compared with those of reference [2], where the wedge was modelled with stepping lined duct sections. For $\Theta_0 = 2\pi$ and small cylinder diameters $2a$ (possibly combined with $G_c = 0$) the present results can be compared with those of the theory for thin absorbing screens by using Mathieu functions (see reference [5]). The present theory will analytically go over to that of reference [4] when both flanks are rigid.

2. FIELD FORMULATION FOR A LINE SOURCE

With a line source at the co-ordinates r_q, ϑ_q the question immediately arises whether it would be better to place the line source in a zone limit, $r_q = r_i$, or inside a zone. Here it is placed inside a zone $i = s$ with $r_q \neq r_{i-1}$, r_i, mainly for reasons of clarity.

The field formulations are of the form

$$p(r, \vartheta, z) = \sum_{\eta} R_\eta(r) T(\eta\vartheta) Z(k_z z), \tag{2}$$

where the factor $Z(k_z z)$ may be one of the functions $e^{\pm jk_z z}$, $\cos(k_z z)$, $\sin(k_z z)$ or a linear combination thereof with a given wave number k_z. Because $Z(k_z z)$ will appear as a factor in all field representations, one can drop it (like the time factor $e^{j\omega t}$); the only consequence of a value $k_z \neq 0$ will be a modification of the radial wave number $k_0^2 \to k^2 = k_0^2 - k_z^2$. For the numerical examples below it is supposed that for $k_z = 0$, $Z(k_z z) = 1$, for reasons of simplicity (nevertheless the wave number symbol k will be used further). The terms in the sum are orthogonal in the range $0 \leqslant \vartheta \leqslant \Theta_0$ for the forms $\cos(\eta\vartheta)$ (symmetrical modes) and $\sin(\eta\vartheta)$ (antisymmetrical modes) for $T(\eta\vartheta)$ or a linear combination thereof (skew modes), if $\eta = \text{const}(\vartheta)$. The boundary condition at the absorbing flank,

$$Z_0 \mathbf{v}_\vartheta(r, \Theta_0) = \frac{\mathrm{j}}{k_0 r} \frac{\partial p(r, \Theta_0)}{\partial \vartheta} \stackrel{!}{=} G p(r, \Theta_0), \tag{3}$$

leads to

$$\begin{aligned} &(\eta\Theta_0)\tan(\eta\Theta_0) = \mathrm{j}kr\Theta_0 G, && \text{symmetrical modes,} \\ &(\eta\Theta_0)\cot(\eta\Theta_0) = -\mathrm{j}kr\Theta_0 G, && \text{antisymmetrical modes.} \end{aligned} \tag{4}$$

These are the characteristic equations for the azimuthal wave numbers η. The solutions η_n generally become functions of r, when $G \neq 0 = \text{const}$ or $|G| \neq \infty$. That is the reason why the wave equation cannot be separated. If however $G = G(r) \sim 1/r$, then $\eta = \text{const}(r)$ and the wave equation leads to the Bessel differential equation for the radial term $R_\eta(r)$,

$$\left(\frac{\partial^2}{\partial r^2} + \frac{1}{r}\frac{\partial}{\partial r} + k^2 - \frac{\eta_n^2}{r^2}\right) R_{\eta_n}(r) = 0, \tag{5}$$

with general solutions of the form

$$R_\eta(r) = R_n(kr) = c_n \mathrm{H}^{(1)}_{\eta_n}(kr) + d_n \mathrm{H}^{(2)}_{\eta_n}(kr), \tag{6}$$

where $\mathrm{H}^{(i)}_{\eta_n}(kr)$ are Hankel functions, propagating radially inward for $i = 1$ and outward for $i = 2$. They have the orders η_n which—according to equation (4)—generally are complex. The counting index n of the modes, which corresponds to the counting of the solutions η_n, is somewhat arbitrary; one can retain $n = 0, 1, 2, \ldots$.

With $G = G(r) = c/r$ with a constant c (having the dimension of a length), the characteristic equations (4) take the forms $z\tan(z) = \mathrm{j}kc\Theta_0$ and $z\cot(z) = -\mathrm{j}kc\Theta_0$, respectively. These are the forms of the characteristic equations for symmetrical and antisymmetrical modes in straight silencer ducts with a locally absorbing lining. The techniques of their solution can be taken from there (see also reference [1]).

A surface admittance $G = G(r) = c/r$ of the corner flank with $c = \text{const}$ over the whole length of the flank would be unrealistic. However one can subdivide the flank into strips of a width Δr and suppose for each strip $r_{i-1} \leqslant r \leqslant r_i$ a surface admittance $G_i(r) = c_i/r$. When one chooses c_i so that the average $\langle G_i(r) \rangle = G$, one obtains the admittance profiles (1). Each of the ring-shaped zones $r_{i-1} \leqslant r \leqslant r_i$ has

its own set of model solutions $\eta_{i,n}$, and the wedge modes in the zones are orthogonal with norms

$$N_{i,n} = \frac{1}{\Theta_0} \int_0^{\Theta_0} \cos^2(\eta_{i,n}\vartheta)\, \mathrm{d}\vartheta = \frac{1}{2}\left(1 + \frac{\sin(2\eta_{i,n}\Theta_0)}{2\eta_{i,n}\Theta_0}\right). \tag{7}$$

The orthogonality of the modes makes possible a modal analysis of the total sound field in which the sound fields of the zones are fitted to each other at the zone limits by their sound pressure and radial velocity. The modal analysis is exact in the sense of a Fourier analysis.

The critical question of the approximation is whether the model with the stepped flank admittance is an acceptable model for the flank with constant G. Here one can trust the often made experience that a surface with a "structured" admittance $G(r)$ can be approximated by a constant admittance if, first, the average $\langle G(r)\rangle$ agrees with G, and, second, if the structure length Δr is small compared to the wave length, and, third, if the variation of $G(r)$ is not too strong (high peaks in $|G(r)|$ would act as isolated scatterers). These conditions can be complied with by the choice of equation (1) and of sufficiently small intervals Δr, except very near to the origin. The neighbourhood of the origin is eliminated by the absorbing cylinder. Even when this has a small radius a, the fulfilment of the conditions can be improved by taking smaller Δr near the origin than at greater distances.

So the characteristic equations for the mode solutions are ($i = 1, 2, \ldots$)

$$(\eta_{i,m}\Theta_0)\begin{cases}\tan\\ \cot\end{cases}(\eta_{i,m}\Theta_0) = \pm \mathrm{j}\Theta_0 \frac{k_0 \Delta r}{\ln(r_i/r_{i-1})} G \begin{cases}\text{rigid}\\ \text{soft}\end{cases} \quad \text{flank at } \vartheta = 0. \tag{8}$$

It should be noticed that $\ln(r_i/r_{i-1}) \to 0$ for large r_i; the solutions tend to those for a soft flank $\eta_{i,m}\Theta_0 \to (m \pm 1/2)\pi$ if the flank at $\vartheta = 0$ is rigid and $\eta_{i,m}\Theta_0 \to m\pi$ if the flank at $\vartheta = 0$ is soft.

The sound field in the zone $i \neq s$ (not containing the source) is formulated as

$$p_i(r, \vartheta) = \sum_{m \geqslant 0} [A_{i,m} \mathrm{H}^{(1)}_{\eta_{i,m}}(kr) + B_{i,m} \mathrm{H}^{(2)}_{\eta_{i,m}}(kr)] \cos(\eta_{i,m}\vartheta),$$

$$Z_0 v_{r,i} = \frac{\mathrm{j}k}{k_0} \sum_{m \geqslant 0} [A_{i,m} \mathrm{H}'^{(1)}_{\eta_{i,m}}(kr) + B_{i,m} \mathrm{H}'^{(2)}_{\eta_{i,m}}(kr)] \cos(\eta_{i,m}\vartheta): \tag{9}$$

i.e., with radially inward and outward going modes. In principle this formulation is retained also behind the source, because reflected waves from the zone steps there could be possible. If however the zone i is far behind the source where the steps become negligibly small the inward running terms with $A_{i,m}$ can be neglected (see below for more about this).

One needs coupling coefficients between modes of adjacent zones given by the integrals ($T_{i,m}(\vartheta)$ are the azimuthal mode functions)

$$X^{(i)}_{m,n} = \frac{1}{\Theta_0}\int_0^{\Theta_0} T_{i,m}(\vartheta)T_{i+1,n}(\vartheta)\,\mathrm{d}\vartheta,$$

$$Y^{(i)}_{m,n} = \frac{1}{\Theta_0}\int_0^{\Theta_0} T_{i,m}(\vartheta)T_{i-1,n}(\vartheta)\,\mathrm{d}\vartheta = X^{(i-1)}_{n,m}. \tag{10}$$

If the flank at $\vartheta = 0$ is rigid, these become

$$X^{(i)}_{m,n} = \frac{1}{2}\left[\frac{\sin((\eta_{i,m}-\eta_{i+1,n})\Theta_0)}{(\eta_{i,m}-\eta_{i+1,n})\Theta_0} + \frac{\sin((\eta_{i,m}+\eta_{i+1,n})\Theta_0)}{(\eta_{i,m}+\eta_{i+1,n})\Theta_0}\right],$$

$$Y^{(i)}_{m,n} = \frac{1}{2}\left[\frac{\sin((\eta_{i,m}-\eta_{i-1,n})\Theta_0)}{(\eta_{i,m}-\eta_{i-1,n})\Theta_0} + \frac{\sin((\eta_{i,m}+\eta_{i-1,n})\Theta_0)}{(\eta_{i,m}+\eta_{i-1,n})\Theta_0}\right], \tag{11a}$$

and, if the flank at $\vartheta = 0$ is soft

$$X^{(i)}_{m,n} = \frac{1}{2}\left[\frac{\sin((\eta_{i,m}-\eta_{i+1,n})\Theta_0)}{(\eta_{i,m}-\eta_{i+1,n})\Theta_0} - \frac{\sin((\eta_{i,m}+\eta_{i+1,n})\Theta_0)}{(\eta_{i,m}+\eta_{i+1,n})\Theta_0}\right],$$

$$Y^{(i)}_{m,n} = \frac{1}{2}\left[\frac{\sin((\eta_{i,m}-\eta_{i-1,n})\Theta_0)}{(\eta_{i,m}-\eta_{i-1,n})\Theta_0} - \frac{\sin((\eta_{i,m}+\eta_{i-1,n})\Theta_0)}{(\eta_{i,m}+\eta_{i-1,n})\Theta_0}\right]. \tag{11b}$$

Consider first the boundary condition at the cylinder around the corner, $r = a$:

$$Z_0 v_r = \frac{\mathrm{j}}{k_0}\frac{\partial p}{\partial r} \stackrel{!}{=} -G_c p. \tag{12a}$$

This gives

$$\frac{\mathrm{j}k}{k_0}[A_{1,m}\mathrm{H}'^{(1)}_{\eta_{1,m}}(ka) + B_{1,m}\mathrm{H}'^{(2)}_{\eta_{1,m}}(ka)] = -G_c[A_{1,m}\mathrm{H}^{(1)}\eta_{1,m}(ka) + B_{1,m}\mathrm{H}^{(2)}_{\eta_{1,m}}(ka)], \tag{12a}$$

leading to

$$B_{1,m} = -A_{1,m}\frac{G_c\mathrm{H}^{(1)}_{\eta_{1,m}}(ka) + \mathrm{j}(k/k_0)\mathrm{H}'^{(1)}_{\eta_{1,m}}(ka)}{G_c\mathrm{H}^{(2)}_{\eta_{1,m}}(ka) + \mathrm{j}(k/k_0)\mathrm{H}'^{(2)}_{\eta_{1,m}}(ka)}, \tag{13}$$

This could also be written $B_{1,m} = r_{1,m}A_{1,m}$ with modal reflection factors $r_{1,m}$

$$r_{1,m} = -\frac{G_c\mathrm{H}^{(1)}_{\eta_{1,m}}(ka) + \mathrm{j}(k/k_0)\mathrm{H}'^{(1)}_{\eta_{1,m}}(ka)}{G_c\mathrm{H}^{(2)}_{\eta_{1,m}}(ka) + \mathrm{j}(k/k_0)\mathrm{H}'^{(2)}_{\eta_{1,m}}(ka)}. \tag{14}$$

It should be noticed that in the zone $i = 1$ only one set of amplitudes is unknown, the set of the $A_{1,m}$.

Consider next the boundary conditions at a zone limit r_i between two zones i and $i + 1$ not containing the source. When one applies the integral

$$\frac{1}{\Theta_0}\int_0^{\Theta_0} \cdots \cos(\eta_{i,m}\vartheta)\,\mathrm{d}\vartheta, \tag{15a}$$

the continuity of the sound pressure gives

$$[A_{i,m}\mathrm{H}^{(1)}_{\eta_{i,m}}(kr_i) + B_{i,m}\mathrm{H}^{(2)}_{\eta_{i,m}}(kr_i)]N_{i,m} = \sum_{n \geqslant 0}[A_{i+1,n}\mathrm{H}^{(1)}_{\eta_{i+1,n}}(kr_i) + B_{i+1,n}\mathrm{H}^{(2)}_{\eta_{i+1,n}}(kr_i)]X^{(i)}_{m,n}, \tag{16a}$$

and the continuity of the radial particle velocity gives

$$[A_{i,m}\mathrm{H}'^{(1)}_{\eta_{i,m}}(kr_i) + B_{i,m}\mathrm{H}'^{(2)}_{\eta_{i,m}}(kr_i)]N_{i,m} = \sum_{n \geqslant 0}[A_{i+1,n}\mathrm{H}'^{(1)}_{\eta_{i+1,n}}(kr_i) + B_{i+1,n}\mathrm{H}'^{(2)}_{\eta_{i+1,n}}(kr_i)]X^{(i)}_{m,n}. \tag{17a}$$

Elimination of the $B_{i,m}$ leads to

$$\begin{aligned} A_{i,m}&[\mathrm{H}^{(1)}_{\eta_{i,m}}(kr_i)\mathrm{H}'^{(2)}_{\eta_{i,m}}(kr_i) - \mathrm{H}'^{(1)}_{\eta_{i,m}}(kr_i)\mathrm{H}^{(2)}_{\eta_{i,m}}(kr_i)]N_{i,m} \\ &= \sum_{n \geqslant 0}[A_{i+1,n}(\mathrm{H}^{(1)}_{\eta_{i+1,n}}(kr_i)\mathrm{H}'^{(2)}_{\eta_{i,m}}(kr_i) - \mathrm{H}'^{(1)}_{\eta_{i+1,n}}(kr_i)\mathrm{H}^{(2)}_{\eta_{i,m}}(kr_i)) \\ &\quad + B_{i+1,n}(\mathrm{H}^{(2)}_{\eta_{i+1,n}}(kr_i)\mathrm{H}'^{(2)}_{\eta_{i,m}}(kr_i) - \mathrm{H}'^{(2)}_{\eta_{i+1,n}}(kr_i)\mathrm{H}^{(2)}_{\eta_{i,m}}(kr_i))]X^{(i)}_{m,n}. \end{aligned} \tag{18}$$

With the Wronski determinant of Hankel functions

$$W(f_1(z), f_2(z)) = f_1(z)f_2'(z) - f_1'(z)f_2(z), \qquad W(\mathrm{H}^{(1)}_\nu(z), \mathrm{H}^{(2)}_\nu(z)) = -\frac{4\mathrm{j}}{\pi z}, \tag{19}$$

one gets the following systems of equations which are downwards recursive in i:

$$\begin{aligned} A_{i,m} = \mathrm{j}\frac{\pi k r_i}{4N_{i,m}} \sum_{n \geqslant 0}&[A_{i+1,n}(\mathrm{H}^{(1)}_{\eta_{i+1,n}}(kr_i)\mathrm{H}'^{(2)}_{\eta_{i,m}}(kr_i) - \mathrm{H}'^{(1)}_{\eta_{i+1,n}}(kr_i)\mathrm{H}^{(2)}_{\eta_{i,m}}(kr_i)) \\ &+ B_{i+1,n}(\mathrm{H}^{(2)}_{\eta_{i+1,n}}(kr_i)\mathrm{H}'^{(2)}_{\eta_{i,m}}(kr_i) - \mathrm{H}'^{(2)}_{\eta_{i+1,n}}(kr_i)\mathrm{H}^{(2)}_{\eta_{i,m}}(kr_i))]X^{(i)}_{m,n}, \end{aligned} \tag{20a}$$

$$\begin{aligned} B_{i,m} = -\mathrm{j}\frac{\pi k r_i}{4N_{i,m}} \sum_{n \geqslant 0}&[A_{i+1,n}(\mathrm{H}^{(1)}_{\eta_{i+1,n}}(kr_i)\mathrm{H}'^{(1)}_{\eta_{i,m}}(kr_i) - \mathrm{H}^{(1)}_{\eta_{i,m}}(kr_i)\mathrm{H}'^{(1)}_{\eta_{i+1,n}}(kr_i)) \\ &+ B_{i+1,n}(\mathrm{H}^{(2)}_{\eta_{i+1,n}}(kr_i)\mathrm{H}'^{(1)}_{\eta_{i,m}}(kr_i) - \mathrm{H}^{(1)}_{\eta_{i,m}}(kr_i)\mathrm{H}'^{(2)}_{\eta_{i+1,n}}(kr_i))]X^{(i)}_{m,n}. \end{aligned} \tag{21a}$$

If instead of the integral (15a) one applies the integral

$$\frac{1}{\Theta_0}\int_0^{\Theta_0} \cdots \cos(\eta_{i+1,m}\vartheta)\,\mathrm{d}\vartheta \tag{15b}$$

on the sound pressure condition, one obtains

$$[A_{i+1,m}\mathrm{H}^{(1)}_{\eta_{i+1,m}}(kr_i) + B_{i+1,m}\mathrm{H}^{(2)}_{\eta_{i+1,m}}(kr_i)]N_{i+1,m} = \sum_{n\geqslant 0}[A_{i,n}\mathrm{H}^{(1)}_{\eta_{i,n}}(kr_i) + B_{i,n}\mathrm{H}^{(2)}_{\eta_{i,n}}(kr_i)]X^{(i)}_{n,m}, \tag{16b}$$

and on the radial particle velocity condition

$$[A_{i+1,m}\mathrm{H}'^{(1)}_{\eta_{i+1,m}}(kr_i) + B_{i+1,m}\mathrm{H}'^{(2)}_{\eta_{i+1,m}}(kr_i)]N_{i+1,m} = \sum_{n\geqslant 0}[A_{i,n}\mathrm{H}'^{(1)}_{\eta_{i,n}}(kr_i) + B_{i,n}\mathrm{H}'^{(2)}_{\eta_{i,n}}(kr_i)]X^{(i)}_{n,m}. \tag{17b}$$

Elimination of the $B_{i+1,m}$ and use of the Wronski determinant yields the upwards iterative system of equations

$$A_{i+1,m} = \mathrm{j}\frac{\pi kr_i}{4N_{i+1,m}}\sum_{n\geqslant 0}[A_{i,n}(\mathrm{H}^{(1)}_{\eta_{i,n}}(kr_i)\mathrm{H}'^{(2)}_{\eta_{i+1,m}}(kr_i) - \mathrm{H}'^{(1)}_{\eta_{i,n}}(kr_i)\mathrm{H}^{(2)}_{\eta_{i+1,m}}(kr_i)) + B_{i,n}(\mathrm{H}^{(2)}_{\eta_{i,n}}(kr_i)\mathrm{H}'^{(2)}_{\eta_{i+1,m}}(kr_i) - \mathrm{H}'^{(2)}_{\eta_{i,n}}(kr_i)\mathrm{H}^{(2)}_{\eta_{i+1,m}}(kr_i))]X^{(i)}_{n,m}, \tag{20b}$$

$$B_{i+1,m} = -\mathrm{j}\frac{\pi kr_i}{4N_{i+1,m}}\sum_{n\geqslant 0}[A_{i,n}(\mathrm{H}^{(1)}_{\eta_{i,n}}(kr_i)\mathrm{H}'^{(1)}_{\eta_{i+1,m}}(kr_i) - \mathrm{H}^{(1)}_{\eta_{i+1,m}}(kr_i)\mathrm{H}'^{(1)}_{\eta_{i,n}}(kr_i)) + B_{i,n}(\mathrm{H}^{(2)}_{\eta_{i,n}}(kr_i)\mathrm{H}'^{(1)}_{\eta_{i+1,m}}(kr_i) - \mathrm{H}^{(1)}_{\eta_{i+1,m}}(kr_i)\mathrm{H}'^{(2)}_{\eta_{i,n}}(kr_i))]X^{(i)}_{n,m}, \tag{21b}$$

When one begins with $i = 1$, only the $A_{1,n}$ are symbolic on the right-hand sides; all other terms are numeric. This remains true when we iterate upwards through i. Finally one comes to $i = s - 1$: i.e., to the zone which is before the zone $i = s$ containing the source.

For the zone $i = s$ one must make a special field formulation which subdivides the zone into two sub-zones $(\sigma) = (1)$ with $r_{i-1} \leqslant r < r_q$ and the sub-zone $(\sigma) = (2)$ with $r_q < r \leqslant r_i$:

$$p^{(\sigma)}_s(r,\vartheta) = \sum_{m\geqslant 0}[A^{(\sigma)}_{s,m}\mathrm{H}^{(1)}_{\eta_{s,m}}(kr) + B^{(\sigma)}_{s,m}\mathrm{H}^{(2)}_{\eta_{s,m}}(kr)]\cos(\eta_{s,m}\vartheta),$$

$$Z_0 v^{(\sigma)}_{r,s} = \frac{\mathrm{j}k}{k_0}\sum_{m\geqslant 0}[A^{(\sigma)}_{s,m}\mathrm{H}'^{(1)}_{\eta_{s,m}}(kr) + B^{(\sigma)}_{s,m}\mathrm{H}'^{(2)}_{\eta_{s,m}}(kr)]\cos(\eta_{s,m}\vartheta). \tag{22}$$

Fitting the sound pressure at the limit $r = r_q$ of the sub-zones gives

$$A^{(1)}_{s,m}\mathrm{H}^{(1)}_{\eta_{s,m}}(kr_q) + B^{(1)}_{s,m}\mathrm{H}^{(2)}_{\eta_{s,m}}(kr_q) = A^{(2)}_{s,m}\mathrm{H}^{(1)}_{\eta_{s,m}}(kr_q) + B^{(2)}_{s,m}\mathrm{H}^{(2)}_{\eta_{s,m}}(kr_q), \tag{23}$$

and the boundary condition for the radial particle velocity there requires

$$v_{r,s}^{(2)}(r_q + 0) - v_{r,s}^{(1)}(r_q - 0) \overset{!}{=} \Phi\, \delta(\vartheta - \vartheta_q), \tag{24}$$

with the volume flow density Φ of the line source and the Dirac delta function $\delta(\vartheta - \vartheta_q)$. This can be expanded in wedge modes of the zone s:

$$\delta(\vartheta - \vartheta_q) = \sum_{n \geqslant 0} b_n T_{s,n}(\vartheta) = \sum_{n \geqslant 0} b_n \cos(\eta_{s,n}\vartheta)$$

$$\frac{1}{\Theta_0}\int_0^{\Theta_0} \delta(\vartheta - \vartheta_q) T_{s,m}(\vartheta)\, \mathrm{d}\vartheta = \frac{1}{\Theta_0}\, T_{s,m}(\vartheta_q) = b_m N_{s,m}, \tag{25}$$

where $b_m = (T_{s,m}(\vartheta_q))/(\Theta_0 N_{s,m})$. With this, the boundary condition (24) gives

$$\frac{\mathrm{j}k}{k_0} \cdot \{[A_{s,m}^{(2)} \mathrm{H}_{\eta_{s,m}}^{\prime(1)}(kr_q) + B_{s,m}^{(2)} \mathrm{H}_{\eta_{s,m}}^{\prime(2)}(kr_q)] - [A_{s,m}^{(1)} \mathrm{H}_{\eta_{s,m}}^{\prime(1)}(kr_q) + B_{s,m}^{(1)} \mathrm{H}_{\eta_{s,m}}^{\prime(2)}(kr_q)]\} = Z_0 \Phi b_m. \tag{26}$$

Together with the sound pressure condition one gets

$$A_{s,m}^{(1)} - A_{s,m}^{(2)} = \frac{\pi}{4} k_0 r_q \mathrm{H}_{\eta_{s,m}}^{(2)}(kr_q) Z_0 \Phi b_m, \tag{27a}$$

$$B_{s,m}^{(1)} - B_{s,m}^{(2)} = -\frac{\pi}{4} k_0 r_q \mathrm{H}_{\eta_{s,m}}^{(1)}(kr_q) Z_0 \Phi b_m. \tag{28a}$$

If one introduces the sound pressure $p_Q(0)$ which the line source would produce in the free field at the corner position,

$$p_Q(0) = \tfrac{1}{4} k_0 r_q Z_0 \Phi \mathrm{H}_0^{(2)}(kr_q), \tag{29}$$

one can write

$$A_{s,m}^{(2)} = A_{s,m}^{(1)} - \pi b_m p_Q(0) \frac{\mathrm{H}_{\eta_{s,m}}^{(2)}(kr_q)}{\mathrm{H}_0^{(2)}(kr_q)}, \tag{27b}$$

$$B_{s,m}^{(2)} = B_{s,m}^{(1)} + \pi b_m p_Q(0) \frac{\mathrm{H}_{\eta_{s,m}}^{(1)}(kr_q)}{\mathrm{H}_0^{(2)}(kr_q)}. \tag{28b}$$

Now one must distinguish two cases. In the first case the source is so far from the corner that the admittance steps behind the source are negligible, i.e., one can set $A_{s,m}^{(2)} = 0$ in equation (27) because no inward running reflections comes from outside the source. When one sets $A_{s,m}^{(1)} = A_{i+1,m}$ with $A_{i+1,m}$ the last result of the iteration (20b), then one has in equations (27) an inhomogeneous linear system of equations for the $A_{1,m}$. After its solution all other amplitudes are obtained by insertion. In the other case, when inward directed reflections must be considered behind the source also, one begins the downward iteration (20a), (21a) at a sufficiently large $i = I$, so that the $A_{I+1,m}$ can be neglected. These iterations contain in their right-hand sides only the symbolic quantities $B_{I+1,m}$. Upon ending the downward iteration with $i = s$ and with the identity $A_{i,m} = A_{s,m}^{(2)}$ and $B_{i,m} = B_{s,m}^{(2)}$,

equations (27b) and (28b) are two systems of linear inhomogeneous equations for the two sets of amplitudes $A_{1,m}$ and $B_{I+1,m}$. After they are solved, all other amplitudes are computed by insertion. Thus the task of the field computation with a line source is solved.

In the case of no zone reflections outside the source, i.e., $A^{(2)}_{s,m} = 0$, one can also perform a downward iteration with equations (27b) and (28b) by setting $A^{(1)}_{s,m} = A_{i+1,m}$, $B^{(1)}_{s,m} = B_{i+1,m}$ and using equations (20a) and (21a) until $i = 1$. The $A_{i+1,m}$ then are purely numerical; the $B_{i+1,m}$ are mixed numeric-symbolic with symbolic quantities $B^{(2)}_{s,m}$. The final equations are the relations $B_{1,m} = r_{1,m}A_{1,m}$ with the modal reflection factors $r_{1,m}$ of equation (14). If they are solved for the $B^{(2)}_{s,m}$, then all other amplitudes are obtained by insertion. This downward iteration has numerical advantages as the matrix of the final equations generally is better conditioned than that of the upward iteration.

3. FIELD FORMULATION FOR AN INCIDENT PLANE WAVE

The incident plane wave is generated by letting go $r_q \to \infty$, and at the same time one can set $A^{(2)}_{s,m} = 0$ (i.e., no inward reflections from behind the source). From equations (27) it is deduced that the amplitudes $A^{(1)}_{s,m}$ are determined:

$$A^{(1)}_{s,m} = \pi b_m p_Q(0)\,\frac{\mathrm{H}^{(2)}_{\eta_{s,m}}(kr_q)}{\mathrm{H}^{(2)}_0(kr_q)} = \pi b_m p_Q(0)\,\mathrm{e}^{\mathrm{j}\eta_{s,m}\pi/2}, \tag{30}$$

where for the last relation the asymptotic approximations for Hankel functions are used, and the b_m are given in equation (25). When one iterates equation (20b) (with only symbolic $A_{1,m}$ on the right-hand side) up to $i + 1 = s$ with s chosen sufficiently high to avoid inward reflections from the limit to the zone $s + 1$, setting $A^{(1)}_{s,m} = A_{i+1,m}$ from the iteration, then one obtains with equation (30) a system of linear inhomogeneous equations for the $A_{1,m}$ from which all other amplitudes follow by insertion. (The implicit assumptions made here, that s is high enough to avoid inward reflections from zone steps and r_s is finite on one hand, but r_q within the zone s shall be infinite, can be realized by a very wide last zone $i = s$.) A downward iteration is possible also in which $A_{i+1,m}$ is taken from equation (30) and $B_{i+1,m}$ left symbolic. The final equations for these then again are furnished by the relations $B_{1,m} = r_{1,m}A_{1,m}$ with the modal reflection factors $r_{1,m}$ of equation (14).

4. NUMERICAL EVALUATION

The numerical evaluation begins with the determination of a zone width Δr. It can be referred to the radius $r_0 = a$ of the inner cylinder and called $s = \Delta r/a$. The ratio of the zone admittance $G_i(r)$ in equation (1) to the flank admittance G can be written ($i = 1, 2, \ldots$) as

$$\frac{G_i(r)}{G} = \frac{1}{r/a}\,\frac{s}{\ln\left(1 + \dfrac{s}{1 + (i-1)s}\right)} = \frac{1}{r/a}\,F_i(s), \qquad F_i(s) = \frac{s}{\ln\left(\dfrac{s}{1 + (i-1)s}\right)}, \tag{31}$$

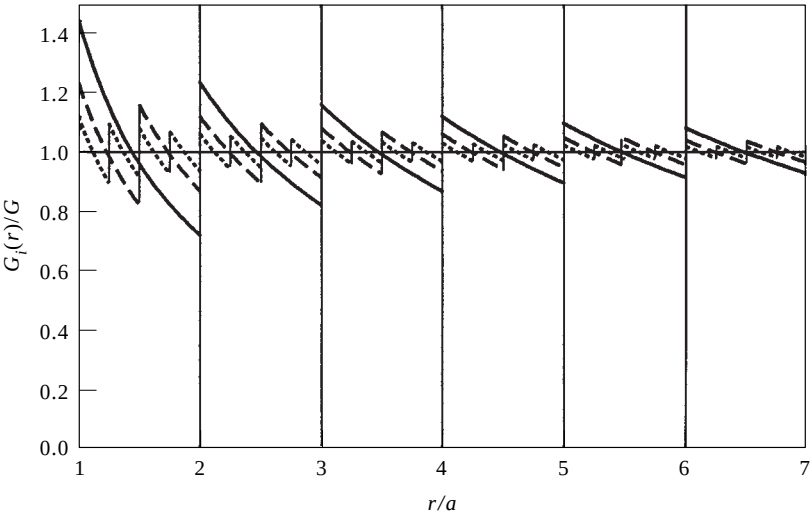

Figure 2. Computed ratios $G_i(r)/G$ for $\Delta r/a = 1$ and $i_{hi} = 6$ (solid line), $\Delta r/a = 0{\cdot}5$ and $i_{hi} = 12$ (long dashes), $\Delta r/a = 0{\cdot}25$ and $i_{hi} = 24$ (short dashes).

and the right-hand side of the characteristic equation (8) becomes $\mathrm{j}\Theta_0 k_0 a G F_i(s)$. The limit of $F_i(s)$ for $s \to 0$ is $F_i(s) \to 1$. A power series expansion of $F_i(s)$ at $s = 0$ begins with

$$F_i(s) \approx 1 + (i - 1/2)s - (1/12)s^2 + \{(i - 1/2)/12\}s^3. \tag{32}$$

The factor $F_i(s)$ is about linear in i and in s for $s < 1$. Figure 2 shows the admittance ratio $G_i(r)/G$ for three step widths: $s = 1$ (solid line); 0·5 (long dashes); 0·25 (short dashes). A step width $s = \Delta r/a = 1$ seems to be a maximum value. Even then the model admittance $G_i(r)$ steps at the first step $i = 1$ only from about $0{\cdot}75G$ to about $1{\cdot}25G$. With $s = 0{\cdot}5$ or smaller the steps between the zones may become negligible for $r/a > 7$.

The characteristic equation (8) with the mode solutions $\eta_{i,m}$ for rigid and absorbing flanks is, with the abbreviation $z_{i,m} = \eta_{i,m}\Theta_0$ of the form

$$z_{i,m} \tan z_{i,m} = \mathrm{j}\Theta_0 k_0 a G F_i(s). \tag{33}$$

It must be solved for a number of zones $i = 1, 2, \ldots, i_{hi}$ and a number of modes $m = 0, 1, \ldots, m_{hi}$. It is convenient to solve it iteratively over i for every m, beginning with $i = 1$ and $F_1(s) \approx 1 + s/2$. A mode-safe algorithm [6] (safe against inadvertent mode jumping during the solution) is used in the first step of the iteration; in higher iterations the solutions from former steps are used as start solutions. For large values of Θ_0 and $k_0 a$ it may be necessary to select a small value for s. Figure 3(a) shows the first six solutions ($m = 0, \ldots, 5$) of $\eta_{i,m}$ in the complex plane for $\Theta_0 = 270^\circ$, $k_0 a = 0{\cdot}5$ with i varying on the curves (indicated by the sampling points) over $i = 1, \ldots, 40$ with a step $s = 0{\cdot}5$. The admittance of the flank is $G = 1 - \mathrm{j}$. The direction on the curves for increasing i is indicated. For large values of i the sampling points lie tight; the surface admittances of neighbour zones in the stepped admittance model become close to each other. In Figure 3(b)

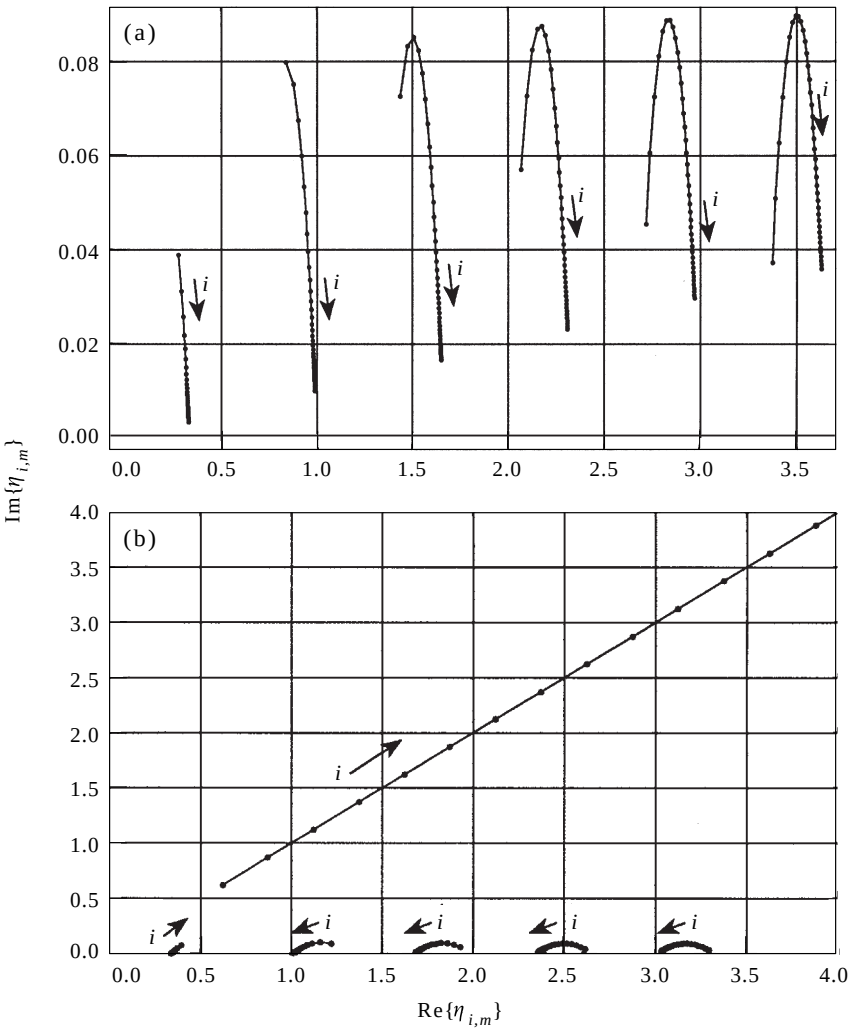

Figure 3. (a) Modal solutions $\eta_{i,m}$ of the modes $m = 0, \ldots, 5$ for increasing $i = 1, \ldots, 40$ with $\Delta r/a = 0{\cdot}5$ and $ka = 0{\cdot}5$ for a corner with $\Theta_0 = 270^\circ$ with normalized admittance $G = 1 - \mathrm{j}$ of the flank. (b) As (a), but with flank admittance $G = 1 + \mathrm{j}$, i.e., with a spring type reactance; the mode $m = 1$ is a surface wave.

only the flank admittance was changed to $G = 1 + \mathrm{j}$ (i.e., with a spring type reactance). The second mode behaves quite differently from the other modes: it is a surface wave; the special role of surface wave modes has been discussed in reference [1]. The $\eta_{i,m}$ are the orders of the Hankel functions in the field formulation. Figures 3(a, b) are typical in showing that—with the exception of the surface wave mode and sometimes the lowest mode—the imaginary component of the order $\eta_{i,m}$ is small compared to its real component.

The order of magnitude of the norms $N_{i,n}$ is about 0·5 and therefore the norms play no role in the convergence of the systems of equations, except the norm of a surface wave mode which can assume very high values. The magnitude of the coupling coefficients $X^{(i)}_{m,n}$ between modes of adjacent zones is easy to describe for

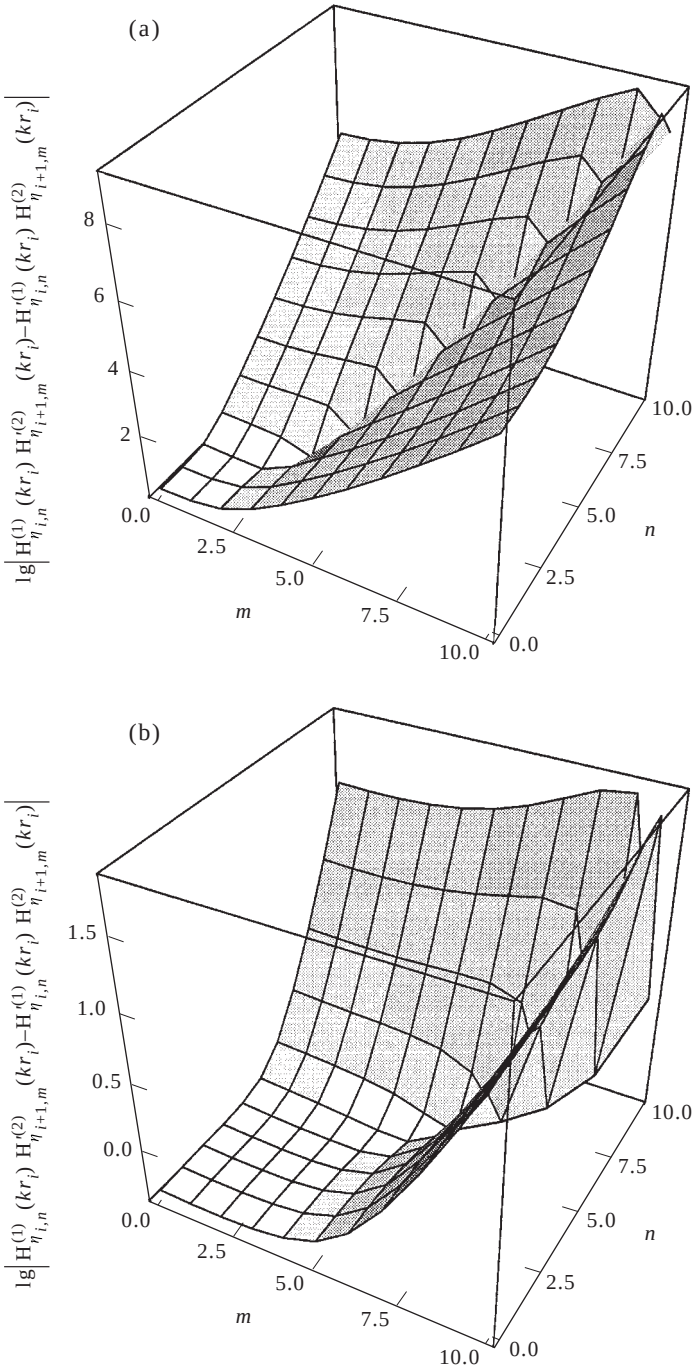

Figure 4—(*Caption on following page*)

modes which are not the surface wave mode. When the steps of the zonal admittance with increasing i become small, the modes of the neighbouring zones more and more approach the behaviour of orthogonal modes; $X^{(i)}_{m,n}$ decreases with

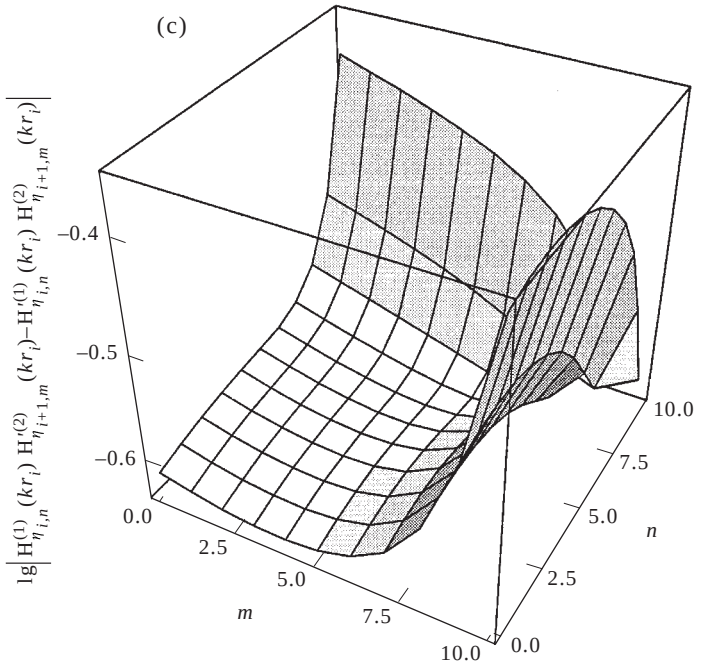

Figure 4. (a) Logarithm of the magnitude of the cross product which is the factor of the $A_{i,n}$ in equation (20b) for the $A_{i+1,m}$; with $kr_i = 0{\cdot}75$; (b) as (a) but with $kr_i = 2{\cdot}75$; (c) as (a) but with $kr_i = 5{\cdot}25$.

an increasing difference in m, n. Therefore the coupling coefficients $X^{(i)}_{m,n}$ produce the convergence of the sums in the systems of equations. The coupling coefficients $X^{(i)}_{m,n}$ become large (especially for high i) if one or both of the modes m, n is a surface wave mode: i.e., when the surface admittance G of the flank has a positive imaginary component. Whereas the sums in the systems of equations for regular modes (not surface wave modes) have a dominant term $m = n$, the situation is not so simple when a surface wave is involved (although the numerical situation is alleviated because only the combination $X^{(i)}_{m,n}/N_{i,m}$ appears in equations (20a), (21a) and $X^{(i)}_{n,m}/N_{i+1,m}$ in equation (20b), (21b)).

The main relations in the determination of the mode amplitudes are the upward recursions (20b), (21b). As mentioned above they will have the shapes

$$A_{i+1,m} = \sum_{n \geqslant 0} a^{(i)}_{m,n} A_{1,n}, \qquad B_{i+1,m} = \sum_{n \geqslant 0} b^{(i)}_{m,n} A_{1,n}, \tag{34}$$

where the $a^{(i)}_{m,n}, b^{(i)}_{m,n}$ are numeric coefficients to the symbolic (i.e., unknown) $A_{1,n}$.

The numerical factors $a^{(i)}_{m,n}, b^{(i)}_{m,n}$ are made up of cross products of Hankel functions. They play a key role in the numerical evaluation. These cross products are not favourable in their magnitude for the convergence of the systems of equations. For small i they may assume large magnitudes outside the main diagonal $m = n$, as Figure 4(a) illustrates with $i = 1$: i.e., $kr_i = 0{\cdot}75$, for the logarithm of the factor of $A_{i,n}$ in equation (20b) for $A_{i+1,m}$. This improves for larger i, as Figure 4(b) shows for $i = 9$, i.e., $kr_i = 2{\cdot}75$, and Figure 4(c) for $i = 19$, i.e.,

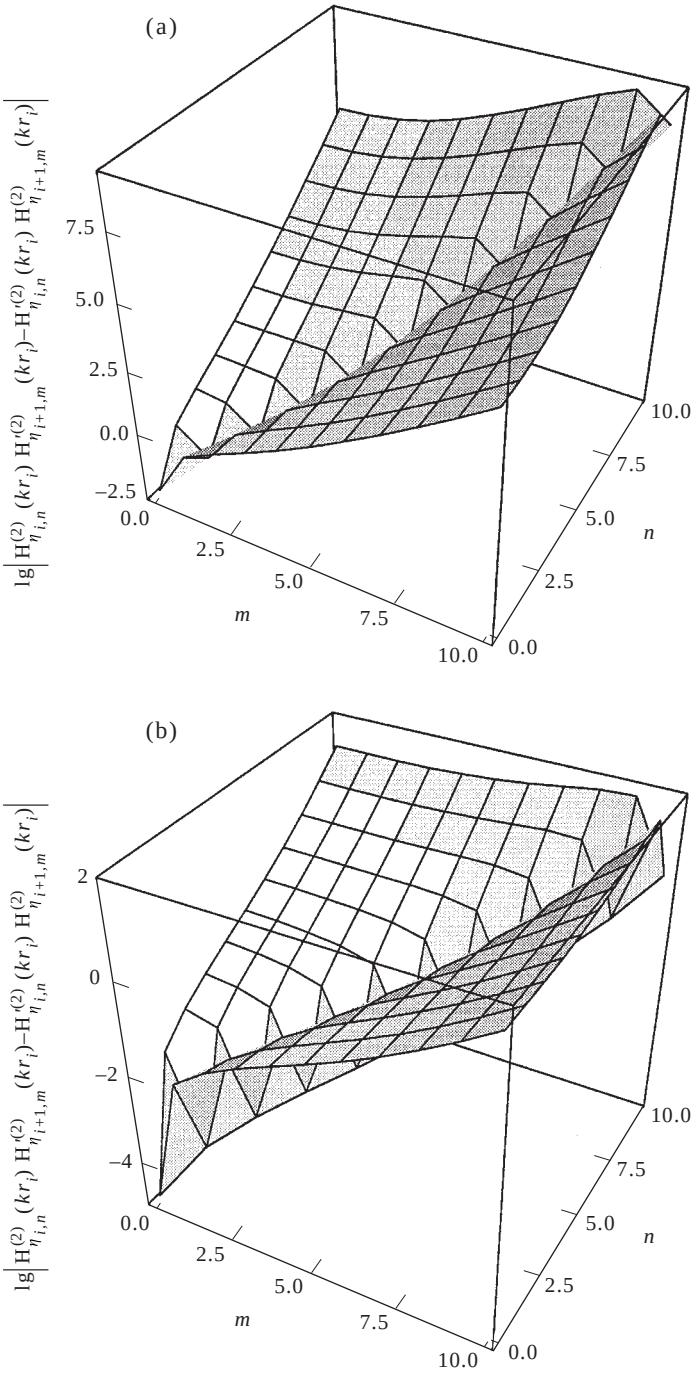

Figure 5—(*Caption on following page*)

$kr_i = 5{\cdot}25$. Figure 5(a–c) show the corresponding factors of $B_{i,n}$ in equation (20b) for $i = 1, 9, 19$, respectively. The other parameters in these diagrams are $k_0 a = 0{\cdot}5$, $\Delta r/a = 0{\cdot}5$, $\Theta_0 = 270^\circ$, $G = 1 - \mathrm{j}$.

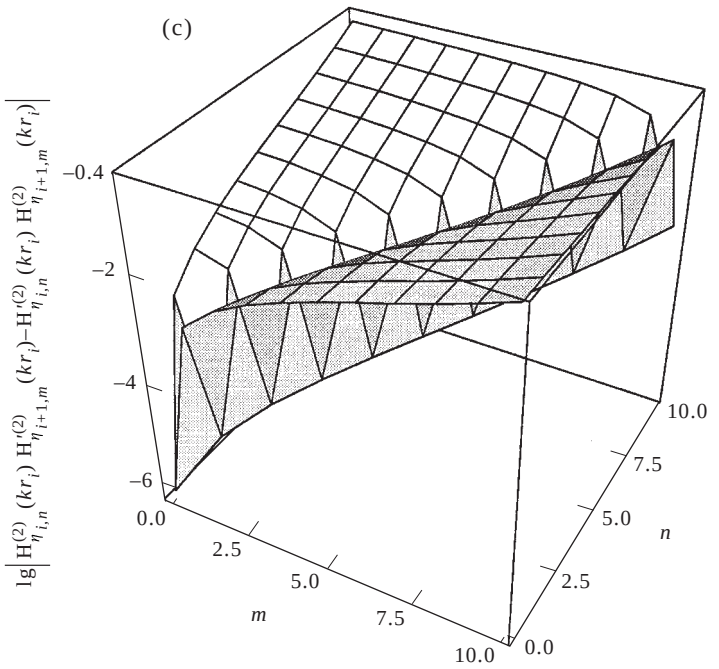

Figure 5. (a) Logarithm of the magnitude of the cross product which is the factor of the $B_{i,n}$ in equation (20b) for the $A_{i+1,m}$, with $kr_i = 0{\cdot}75$; (b) as (a) but with $kr_i = 2{\cdot}75$; (c) as (a) but with $kr_i = 5{\cdot}25$.

For a distant line source, i.e., $A^{(2)}_{s,m} = 0$ in equation (27b), the first relation (with $i + 1 = s$) forms the final system of equations for the $A_{1,n}$ (with $m = 0, 1, \ldots$):

$$A^{(1)}_{s,m} = A_{s,m} = \sum_{n \geqslant 0} a^{(s-1)}_{m,n} A_{1,n} = \pi \frac{\cos(\eta_{s,m}\vartheta_q)}{\Theta_0 N_{s,m}} \frac{H^{(2)}_{\eta_{s,m}}(kr_q)}{H^{(2)}_0(kr_q)} p_Q(0). \tag{35}$$

If the $a^{(i)}_{m,n}$, $b^{(i)}_{m,n}$ are saved during the iteration, the amplitudes $A_{i+1,m}$, $B_{i+1,m}$ follow by insertion with known solutions $A_{1,n}$ of equation (35) (and similarly for downward iterations). All mode amplitudes are proportional to the arbitrary value of $p_Q(0)$, which therefore is set to $p_q(0) = 1$. The procedure of the mixed numeric and symbolic iteration (which easily can be performed with symbolic-numeric programs like *Mathematica*©) has the important advantage that no matrices must be inverted or intermediate systems of equations must be solved during the iteration; the numerical errors remain small, therefore.

The question up to which limits i_{hi}, m_{hi} the zone and mode indices should be applied could be discussed analytically if no surface wave mode is implied; however it is easier to find the limits by numerical experiments. The limit m_{hi} is delicate: if it taken too low, then the mode sums do not yet represent the true field (see examples below); if it is taken too high, then numerical errors in the Hankel functions can make the matrix of the system of equations badly conditioned. The main computational steps are, first, the solution of the characteristic equation for i_{hi} times $m_{hi} + 1$ mode solutions; this can be done within a few minutes. Next, the

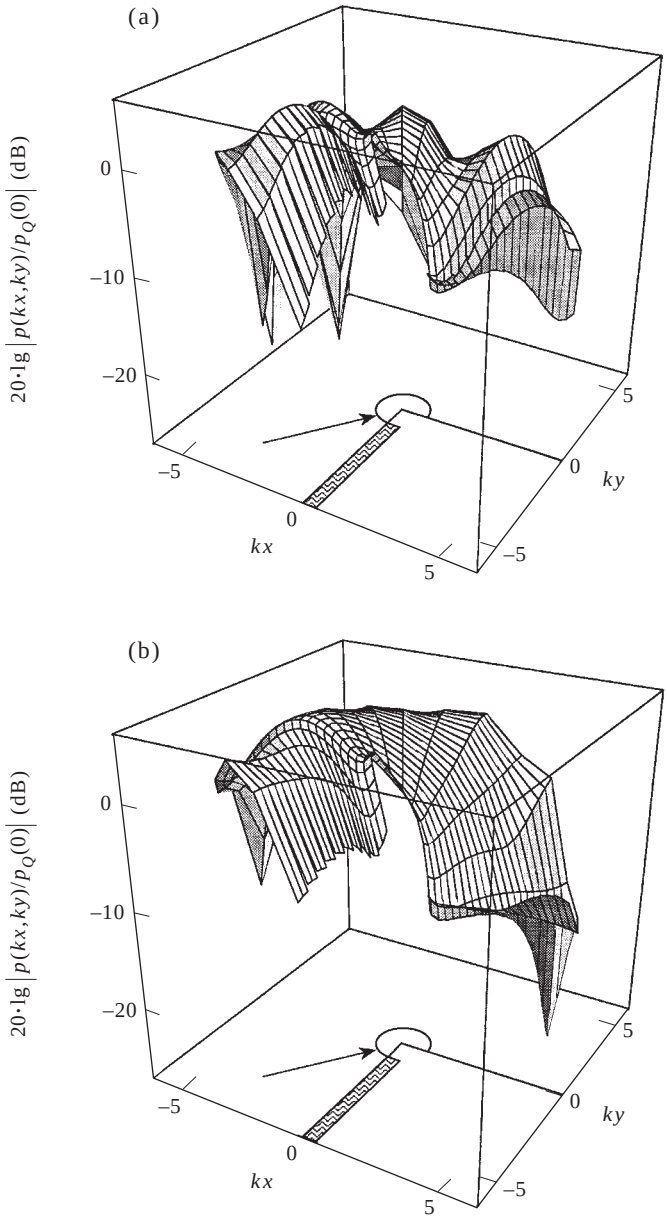

Figure 6—(*Caption on following page*)

evaluation of the norms $N_{i,m}$ and of the coupling coefficients $X^{(i)}_{m,n}$ can be performed also in a short time. And also the mixed numeric-symbolic iteration of the amplitude equations, the solution of the final system of equations and the insertion of the numeric $A_{1,m}$ into the mixed expressions for $A_{i+1,m}$, $B_{i+1,m}$ is finished within some minutes. The longest computing time is consumed by the evaluation of the Hankel functions $H^{(1),(2)}_{n_{i,m}}(kr)$ with complex orders for the field representation; this may take hours (in the computations of this paper the built-in Bessel and

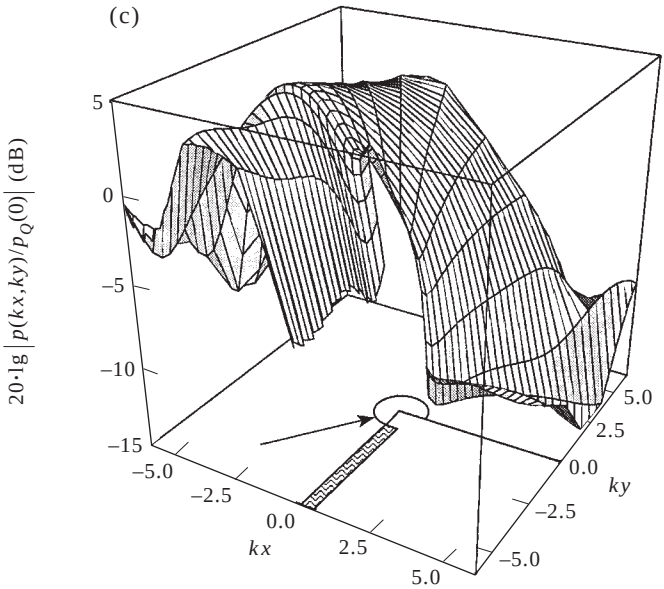

Figure 6. Sound pressure level field around a corner with wedge angle $\Theta_0 = 270^\circ$ and flank admittance $G = 1 - \mathrm{j}$ with an absorbing cylinder of $k_0 a = 1$ and surface admittance $G_c = 1 + 0{\cdot}5\mathrm{j}$ for plane wave incidence with $\vartheta_q = 240^\circ$ (in downward iteration), computed with mode order limit $m_{hi} = 4$ in $i_{hi} = 10$ zones with relative width $s = \Delta r/a = 0{\cdot}5$; (b) as (a) but computed with mode order limit $m_{hi} = 8$; (c) as (a), (b) but computed with mode order limit $m_{hi} = 12$.

Neumann functions in *Mathematica*® were applied which are for complex orders also). The recursive relations for Bessel functions cannot be applied for the fast generation of mode sets of these functions because the orders $\eta_{i,m}$ are not sequences of either integers or simple rationals.

The series of the three-dimensional sound pressure level plots $20 \lg |p(kx, ky)/p_Q(0)|$ in dB of Figure 6(a–c) show the influence of the applied mode numbers m_{hi} in the field computation. The plots are for $m_{hi} = 4$, $m_{hi} = 8$, $m_{hi} = 12$, respectively. The field becomes stationary for about $m_{hi} \approx 10$. The examples are results of downward iterations with a plane wave incident from $\vartheta_q = 240^\circ$ on a right-angled corner, $\Theta_0 = 270^\circ$, with a normalized surface admittance $G = 1 - \mathrm{j}$ of one flank (at $kx = 0$; the other flank at $\vartheta = 0$, i.e., $ky = 0$ being rigid) and a cylinder with $ka = 1$ having a normalized surface admittance $G_c = 1 + 0{\cdot}5\mathrm{j}$ around the corner. The number of zones is $i_{hi} = 10$ with $\Delta r/a = 0{\cdot}5$. The plots are shown with angular steps $\Delta\vartheta = 15^\circ$ and three radial values $(r_{i-1}, 0{\cdot}5(r_{i-1} + r_i), r_i)$ in each zone. The small field gaps between the zones, visible for low m_{hi}, diminish with increasing m_{hi}. This observation is normal for a Fourier synthesis with low numbers of Fourier components. The number of modes in Figure 6(a) with $m_{hi} = 4$ evidently is too small; interference maxima exists in the shadow area of the corner. A higher number of modes, like $m_{hi} = 12$ in Figure 6(c), is necessary to synthesize the monotonic slope of the level profile in the shadow area near the rigid flank both in the radial and in the azimuthal directions. As Figure 6(c) indicates and computations with larger kr range confirm, interference variations appear in the shadow at larger radial distances from the corner and larger azimuthal distances

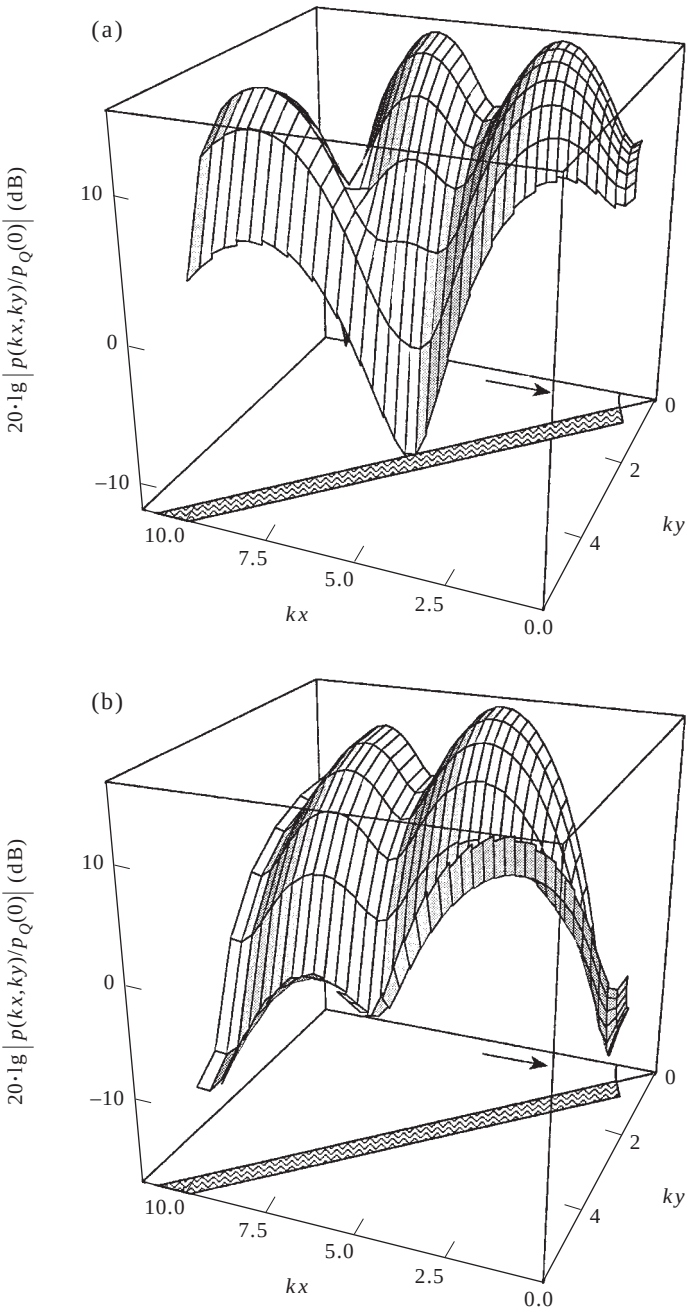

Figure 7. Sound pressure level field in an acute-angled wedge-shaped space with angle $\Theta_0 = 30^\circ$ and flank admittance $G = 1 - 1{\cdot}25\text{j}$, with an absorbing cylinder of $k_0 a = 1$ and surface admittance $G_c = 1 + 0{\cdot}5\text{j}$, for plane wave incidence with $\vartheta_q = 0^\circ$ (in downward iteration), computed with modes of order $m = 0, 1$ in $i_{hi} = 20$ zones with relative width $s = \Delta r/a = 0{\cdot}5$; (b) as (a) but with flank admittance $G = 1 + 1{\cdot}25\text{j}$.

from the rigid flank. These interference variations are the main difference in the level profile produced by the absorption of one flank as compared to two rigid flanks, if the wedge is obtuse-angled. The surface wave mode—although exceptional in its mode wave number—plays no important role in wide wedge spaces, it is only weakly excited there.

The final numerical examples belong to acute-angled wedge spaces with $\Theta_0 = 30^\circ$. In Figures 7(a, b) (which differ only in the sign of the reactance of $G = 1 \pm 1{\cdot}25\text{j}$) a plane wave is incident with $\vartheta_q = 0$, i.e., parallel to the rigid flank towards the wedge apex, which is covered by a cylinder with $k_0 a = 1$ and a surface admittance $G_c = 1 + 0{\cdot}5\text{j}$. Only the wedge modes $m = 0, 1$ can be used. Higher modes in the computation lead to a badly conditioned matrix in the final system of equations. The acoustical reasoning for this finding is as follows: with a (rather) soft flank, i.e., $|G|$ high, the higher modes directed to the apex run through zones with mode cut-off; the errors in the mode fitting between zones would become large. Whereas in Figure 7(a) the mode $m = 1$ is dominant for $kx > 5$, it is practically absent for $kx \leqslant 2{\cdot}5$. In Figure 7(b) with the spring type reactance of the absorbing flank, $G = 1 + 1{\cdot}25\text{j}$, the mode $m = 1$ is a surface wave. Near the wedge apex it is dominent; it produces the steep level slope towards the absorbing flank (which is required by the fit of the field admittance to the flank admittance). Both diagrams show that in acute-angled wedge spaces with an absorbing flank the value of the wall admittance may drastically change the field pattern.

5. CONCLUSION

The method described above for a modal analysis in wedge-shaped spaces with absorbing flanks has the advantage that it is applicable in the full range of the wedge angle Θ_0. However it is numerically tedious. Not only the computation of Bessel and Neumann functions with complex orders is time consuming, but also the right number of the modes involved must be determined by numerical tests. The upward and the downward iterations through the ring-shaped zones of the model generally produce equivalent results. The influence of a finite flank admittance with the obtuse-angled wedges (e.g., building corners or screens) as compared to both flanks rigid mostly is not very pronounced; the sound field in the shadow area shows more variations with absorption than without. This changes for acute-angled wedges; there a finite flank admittance causes zones of cut-off for higher modes, and the sound field pattern accordingly may change rather drastically.

REFERENCES

1. F. P. MECHEL *Journal of Sound and Vibration* In press. Modes in lined wedge-shaped ducts.
2. F. P. MECHEL *Journal of Sound and Vibration* In press. Modal analysis in lined wedge-shaped ducts.
3. F. P. MECHEL *Journal of Sound and Vibration* **219**, 105–132. Scattering at rigid building corners.

4. F. P. MECHEL 1999 *Journal of Sound and Vibration* **219**, 559–579. Improvement of corner shielding by an absorbing cylinder.
5. F. P. MECHEL 1997 *Acta Acustica* **83**, 260–283. A uniform theory of sound screens and dams.
6. F. P. MECHEL 1991 *Acustica* **73**, 223–239. Modal solutions in rectangular ducts lined with locally reacting absorbers.